Supplementary S1

Non-canonical G_q Activation by Orexin Receptor Type 2 and Lemborexant Observed in Microsecond Molecular Dynamics Simulations

*Paulina Dragan[1], Valerie Gratio[2,3], Thierry Voisin[2], Alain Couvineau[2], Dorota Latek[1,]**

[1]University of Warsaw, Faculty of Chemistry, 02-093 Warsaw, Poland

[2]INSERM UMR1149/Inflammation Research Center (CRI), Université Paris Cité, Team "From inflammation to cancer in digestive diseases (INDiD)", DHU UNITY, 75018 Paris, France

[3]INSERM UMR1149/Inflammation Research Center (CRI), Université Paris Cité, Flow cytometry platform (CytoCRI), DHU UNITY, 75018 Paris, France

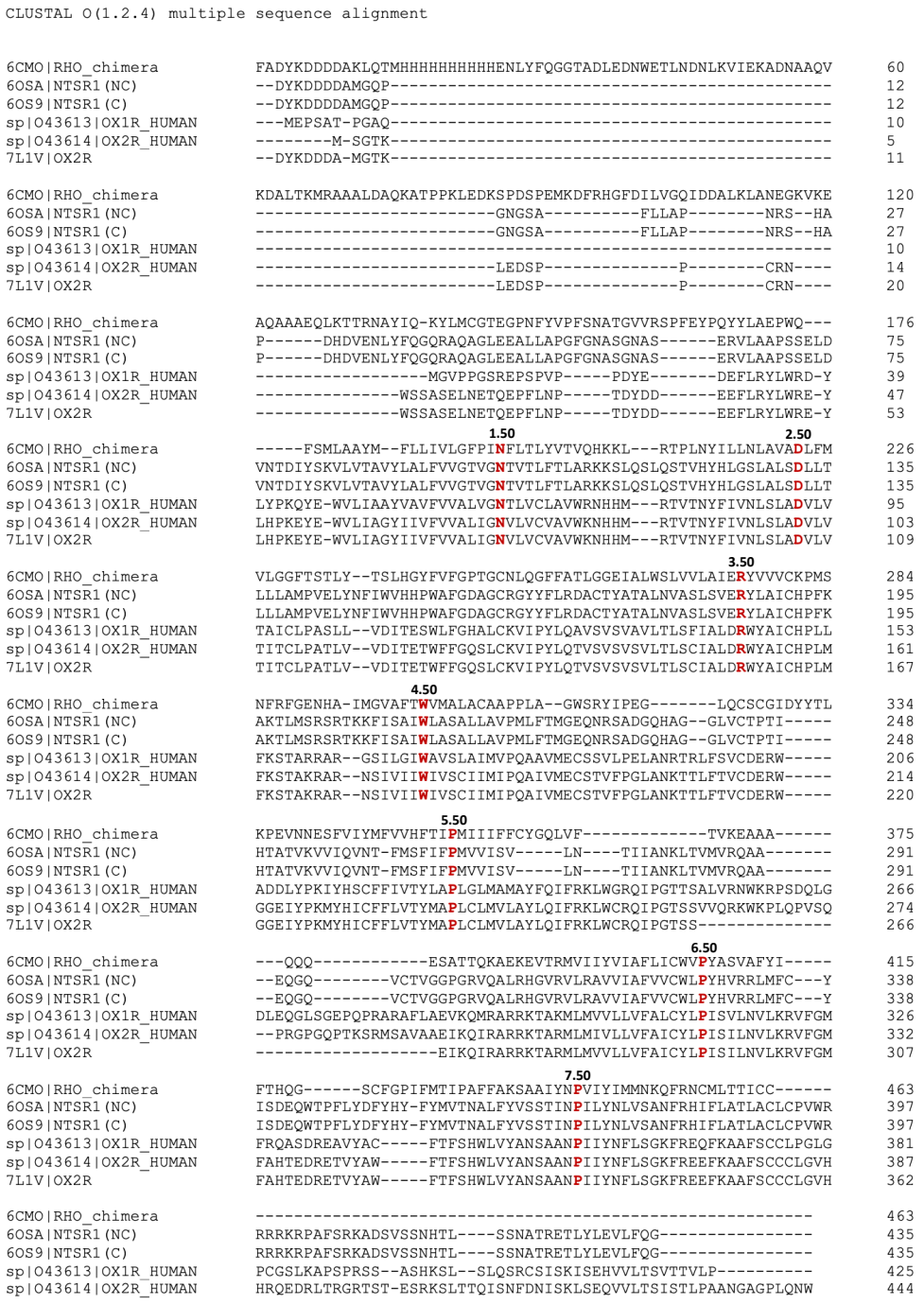

Figure S1. Multiple sequence alignment of OX_1, OX_2 (UniProt ID: O43613, O43614, respectively), NTSR1 (6OSA, 6OS9), and rhodopsin (6CMO). OX_1 and OX_2 sequences were derived from UniProt [1, 2], while the remaining sequences were extracted from PDB structures [3, 4, 5]. The most conserved residues were marked in red and numbered according to the Ballesteros-Weinstein notation [6]. The alignment was performed using Clustal Omega v. 1.2.4.[7].

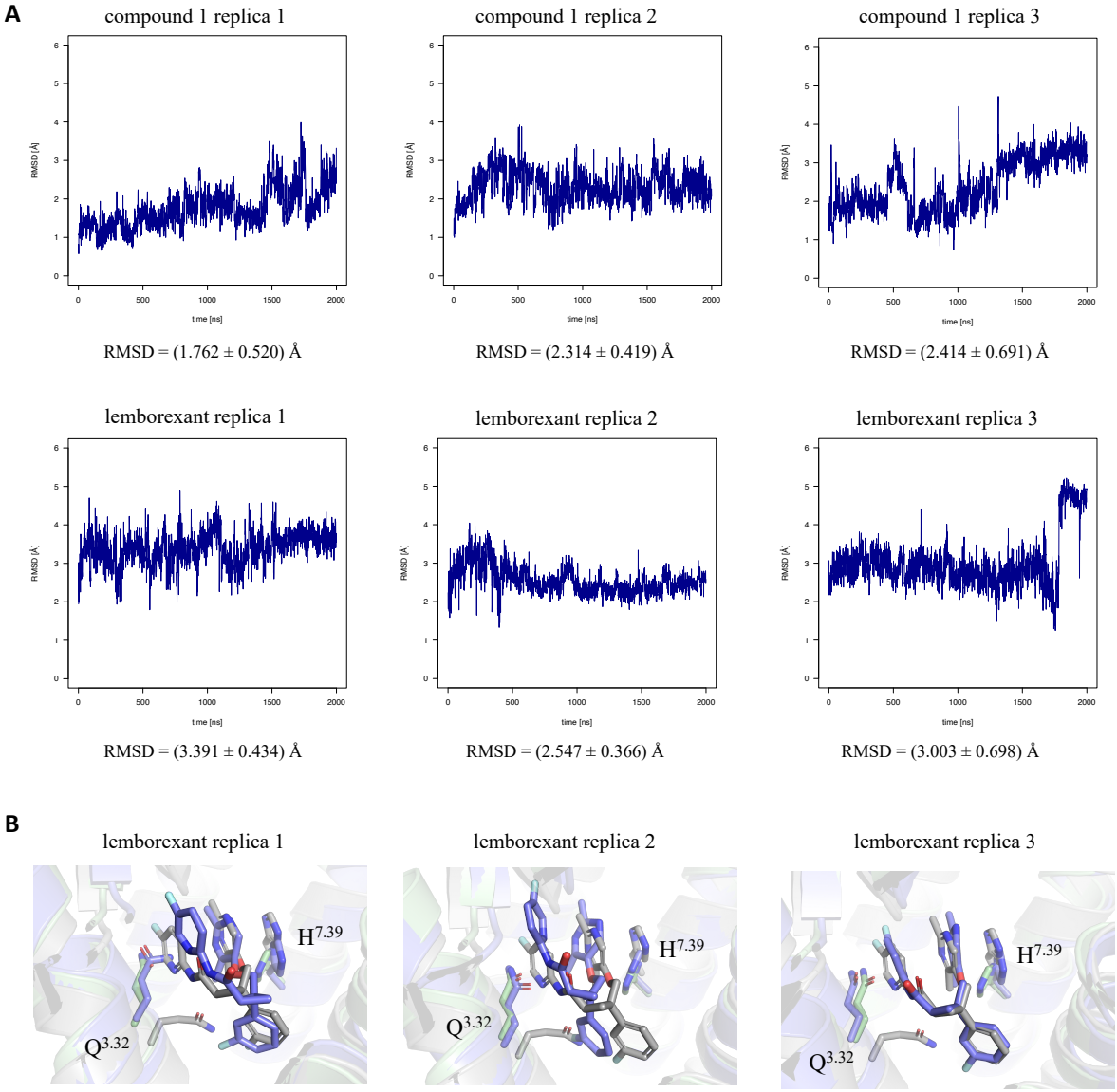

Figure S2. Fluctuations in the binding site area and comparison with PDB structures. (A) The RMSD plots and average RMSD fluctuations obtained for compound 1 and lemborexant-including simulation systems. (B) A superposition of the active-state 7L1V PDB structure (green), the inactive-state 7XRR structure (gray), and the first frame of the lemborexant-including simulations (blue). Residues $Q^{3.32}$ and $H^{7.39}$ are shown as sticks.

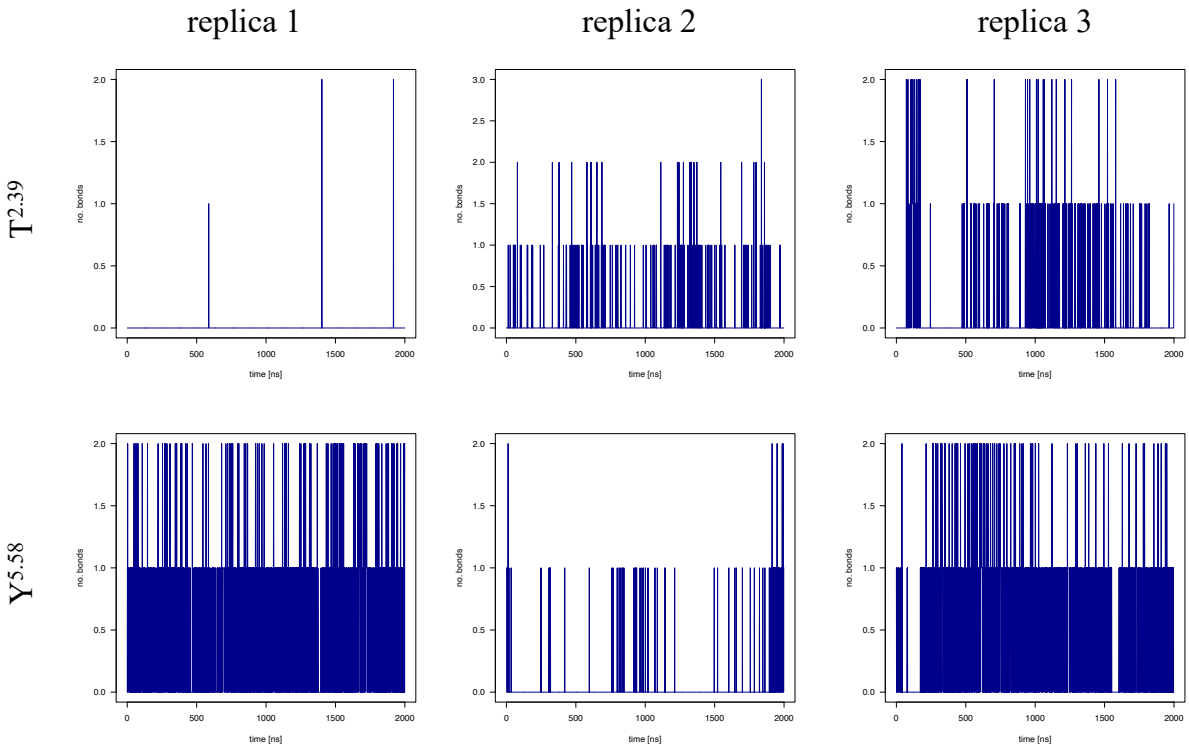

Figure S3. The formation of hydrogen bonds between $R^{3.50}$ of the 'DRW' motif and residues $T^{2.39}$ and $Y^{5.58}$ in the compound 1-including simulations. The 'DRW' motif corresponds to the well-known 'DRY' motif in GPCRs. The maximum hydrogen bond distance was set to 4 Å and the angle cut-off was set to 20º (VMD settings). In orexin receptors, the inactive-state interactions of $R^{3.50}$ are visible in 7XRR (OX2 bound to lemborexant), while the active-state interactions are visible in 7L1U (OX_2 bound to OxB) and 7L1V (OX_2 bound to compound 1).

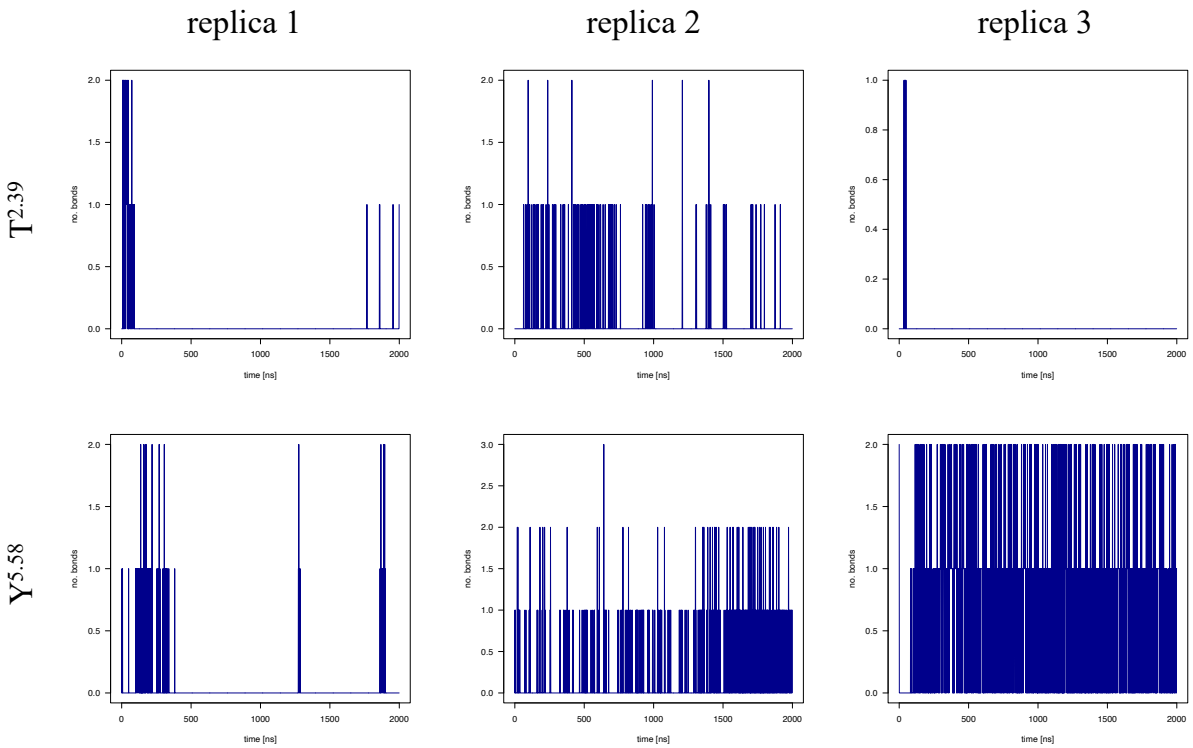

Figure S4. The formation of hydrogen bonds between $R^{3.50}$ of the 'DRW' motif and residues $T^{2.39}$ and $Y^{5.58}$ in the lemborexant-including simulations. The maximum hydrogen bond distance was set to 4 Å and the angle cut-off was set to 20º (VMD typical settings).

A

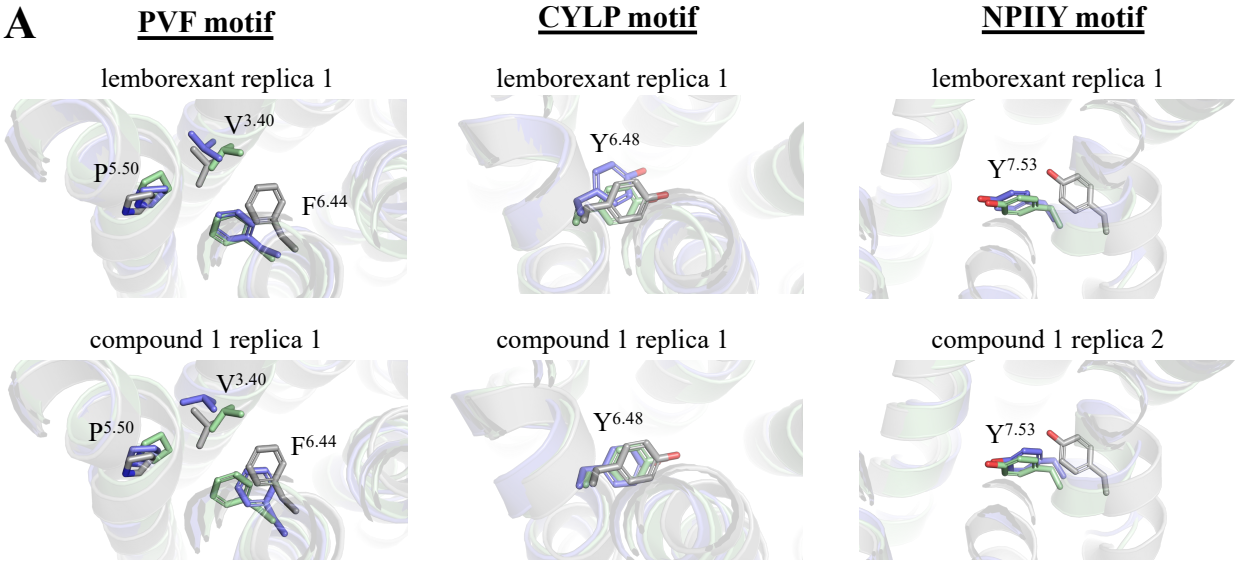

B

motif	lemborexant			compound 1		
	replica 1	replica 2	replica 3	replica 1	replica 2	replica 3
PVF	intermediate	intermediate	intermediate	intermediate	active	intermediate
CYLP	active	active	active	inactive	inactive	active
NPIIY	active	active	active	intermediate	active	active

Figure S5. A comparison of conformations of sequence motifs in simulations systems and in PDB structures. (A) A comparison of the PIF (PVF in OX_2), CWxP (CYLP in OX_2), and NPxxY (NPIIY in OX_2) microswitches in the active-state 7L1V structure (green), inactive-state 7XRR structure (gray), and the final frame of the simulation replicas (blue). (B) A table describing the conformations of the microswitches in the final frame for each replica.

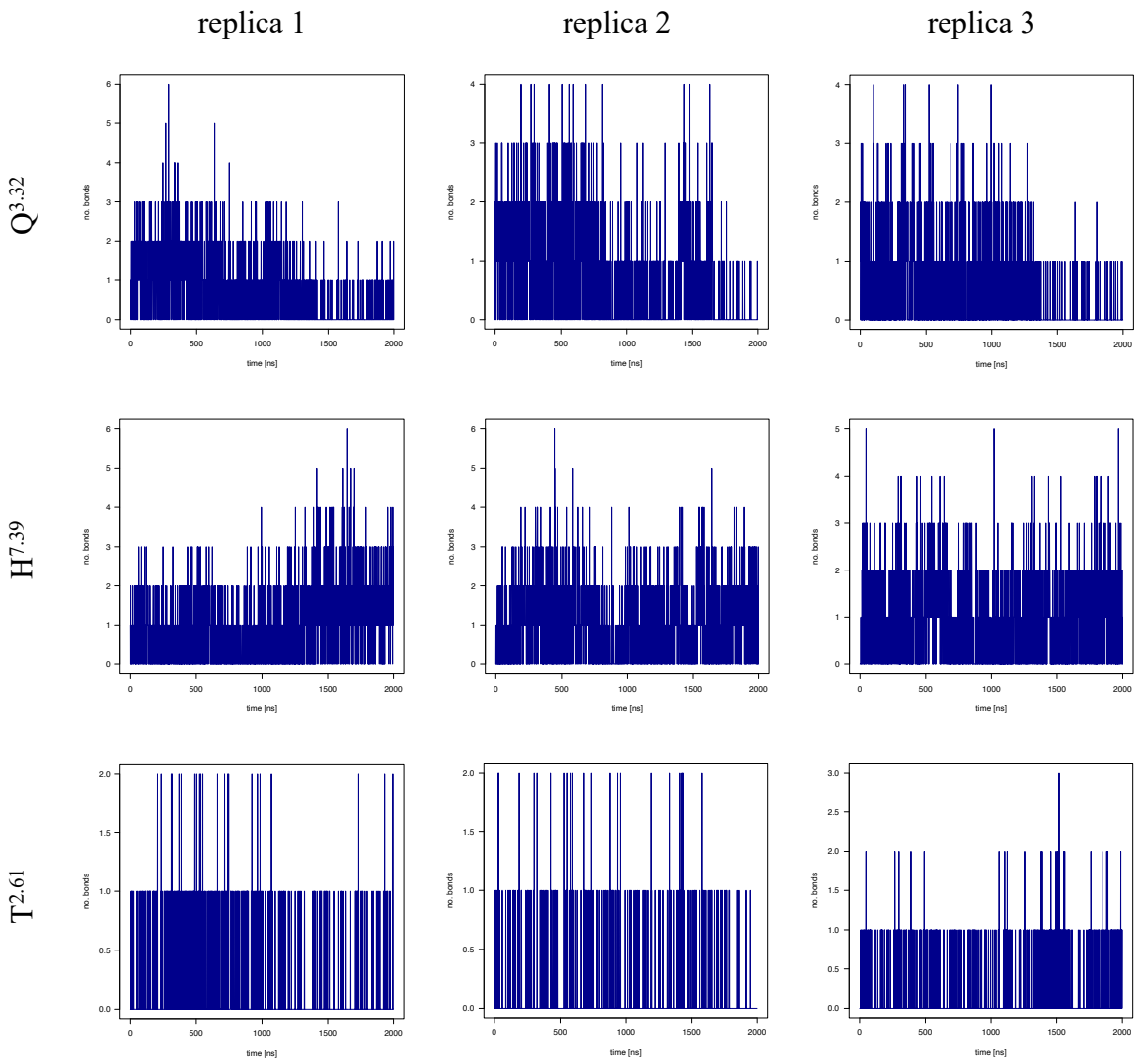

Figure S6. The formation of hydrogen bonds between compound 1 and the OX_2 receptor residues $Q^{3.32}$, $H^{7.39}$, and $T^{2.61}$. The maximum hydrogen bond distance was set to 4 Å, and the angle cut-off was set 20º (VMD settings). According to Hong et al., a hydrogen bond should be present between $H^{7.39}$ and the amide carbonyl linker of compound 1, and further contacts with this residue stabilized the bent conformation of the ligand [3].

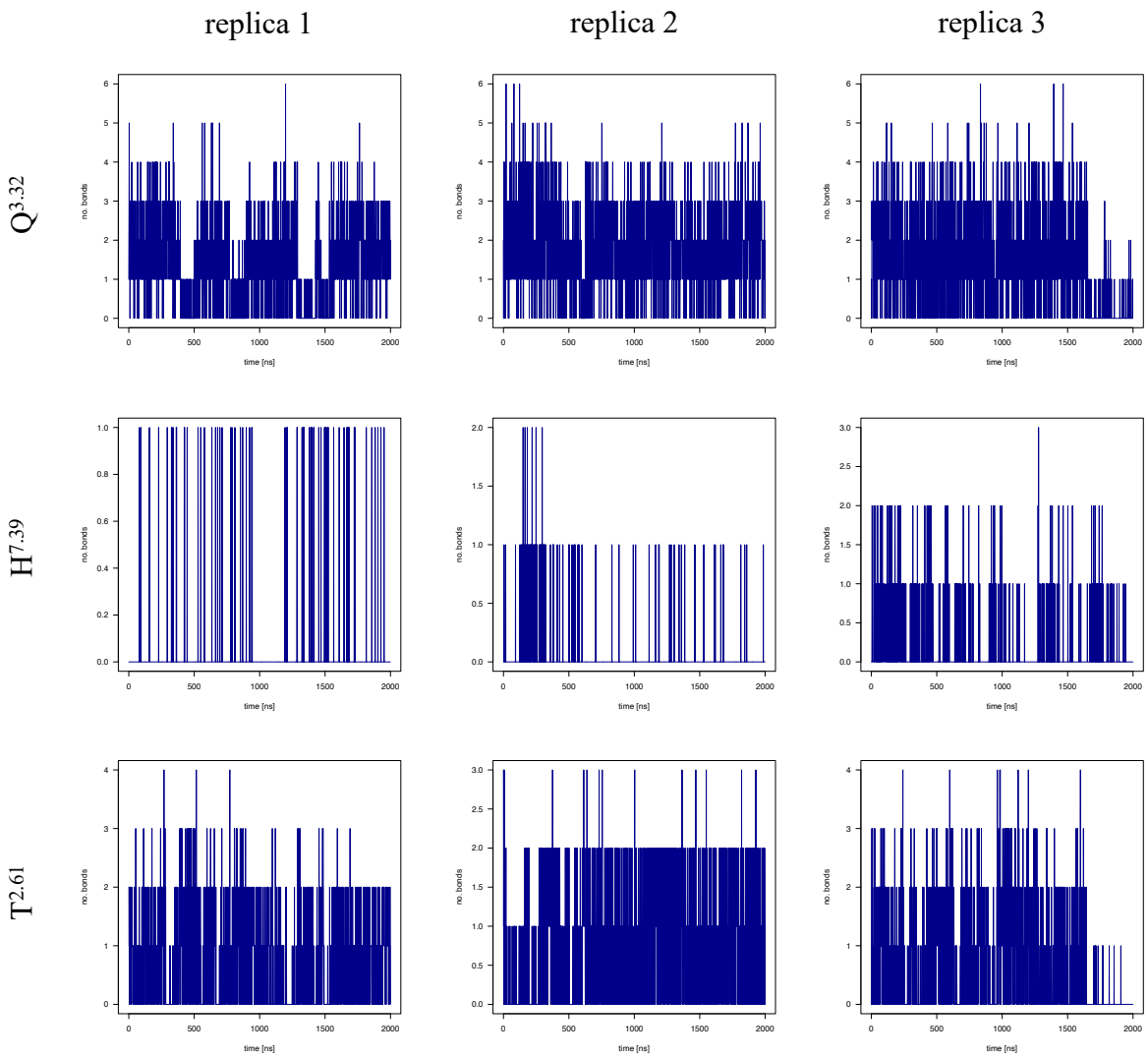

Figure S7. The formation of hydrogen bonds between lemborexant and the OX_2 receptor residues $Q^{3.32}$, $H^{7.39}$, and $T^{2.61}$. The maximum hydrogen bond distance was set to 4 Å, and the angle cut-off was set 20º (VMD typical settings).

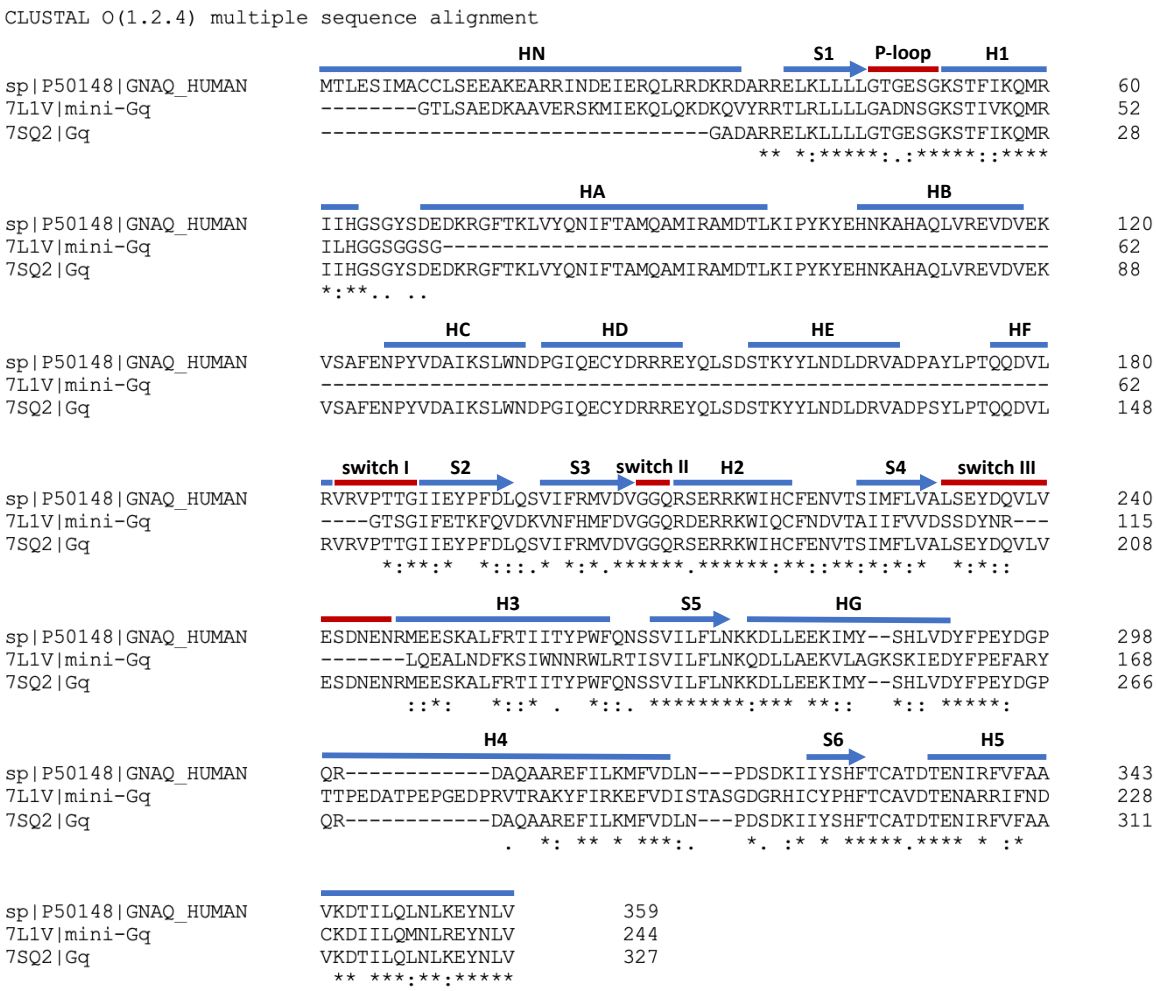

Figure S8. Multiple sequence alignment of Gα$_q$ (UniProt ID: P50148) and Gα subunits in the 7L1V and 7SQ2 PDB structures. The first Gα$_q$ sequence was derived from UniProt [8] and following Gα sequences from 7L1V [3] and 7SQ2 [9] PDB structures, respectively. Residues were assigned a secondary structure based on the GproteinDb [10] numbering for Gα$_q$ and the topology of the Gα subunit described by Calebiro et al. [11] The multiple sequence alignment was performed using Clustal Omega v. 1.2.4. [12].

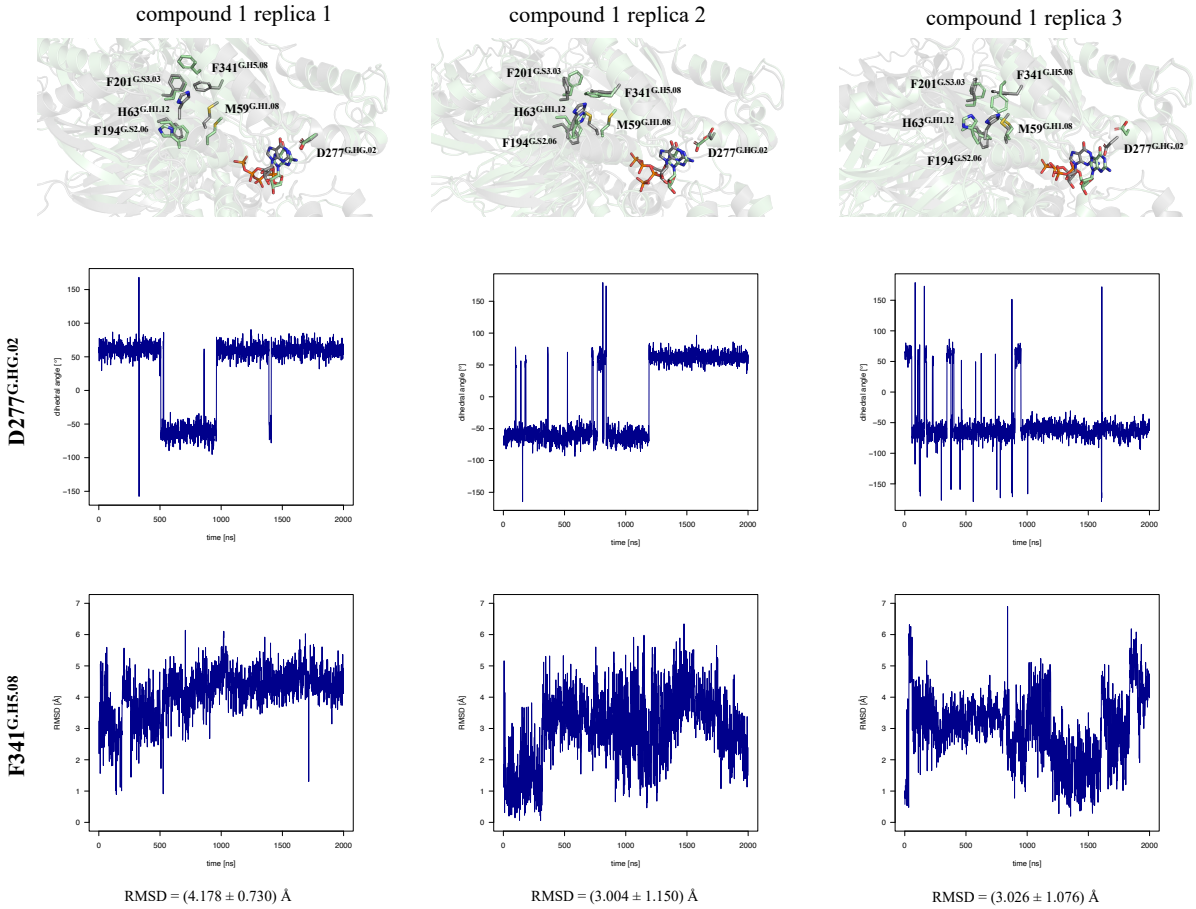

Figure S9. Changes of the D277 (D272) and F341 (F336) microswitches conformations observed in the compound 1-including simulations. (**Top**) Changes in the conformation of the microswitches between the first (gray) and the last (green) frame of the compound 1-including simulations. (**Middle**) The χ1 dihedral angle (N–C_α–C_β–C_γ) computed for microswitch $D277^{G.HG.02}$ (ca. -60°—on; 60°—off). (**Bottom**) The RMSD graphs and mean RMSD values computed for a single carbon atom of the phenyl group of microswitch $F341^{G.H5.08}$. $D277^{G.HG.02}$ and $F341^{G.H5.08}$ refer to D272 and F336 as labeled by Ham et al. [13].

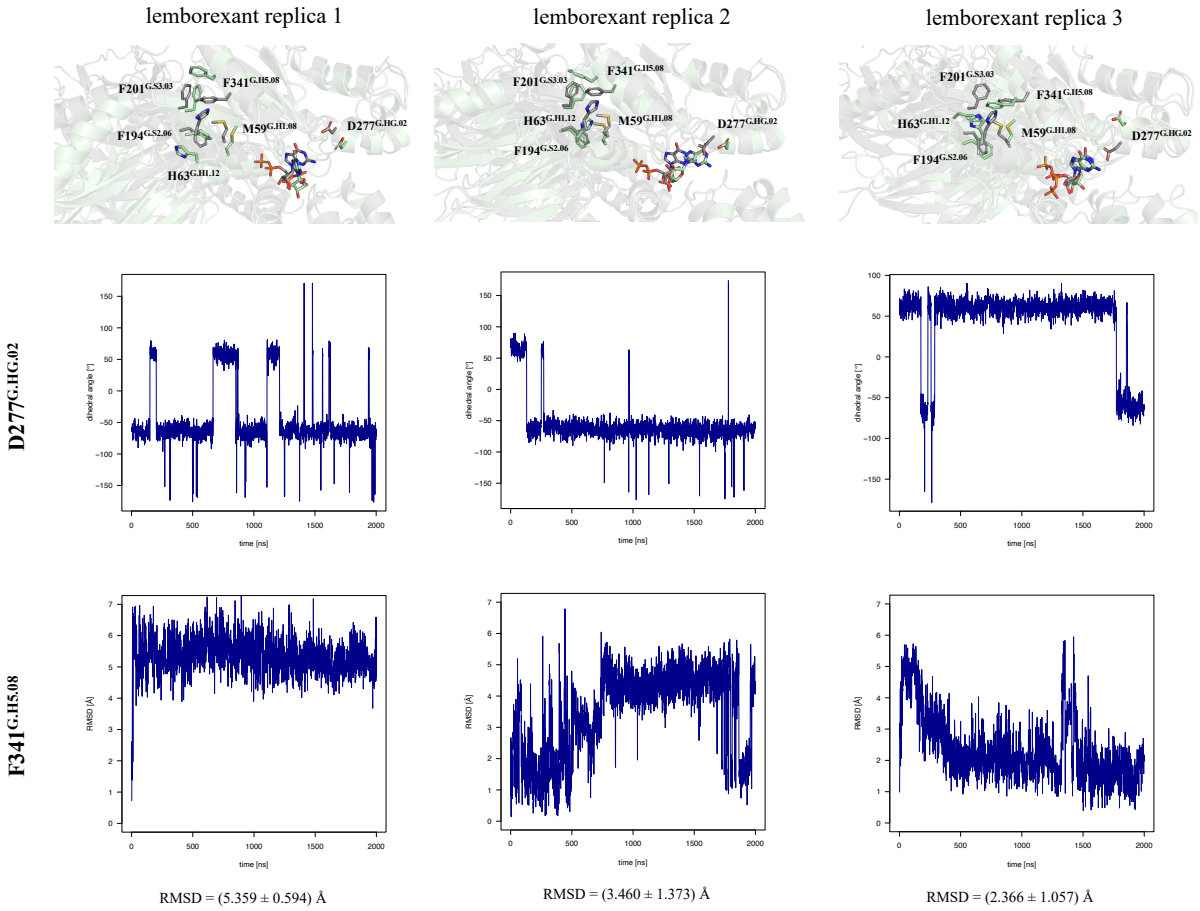

Figure S10. Changes of the D227 (D272) and F341 (F336) microswitches conformations observed in the lemborexant-including simulations. (**Top**) The changes in the conformations of the microswitches between the first (gray) and the last (green) frame of the lemborexant-including simulations. (**Middle**) The dihedral angle between the nitrogen and carbon atoms of the main chain and the two carbon atoms of the side chain computed for microswitch D277$^{G.HG.02}$ (ca. -60°—on; 60°—off). (**Bottom**) The RMSD graphs and mean RMSD values computed for a single carbon atom of the phenyl group of microswitch F341$^{G.H5.08}$. D277$^{G.HG.02}$ and F341$^{G.H5.08}$ refer to D272 and F336 as labeled by Ham et al. [13].

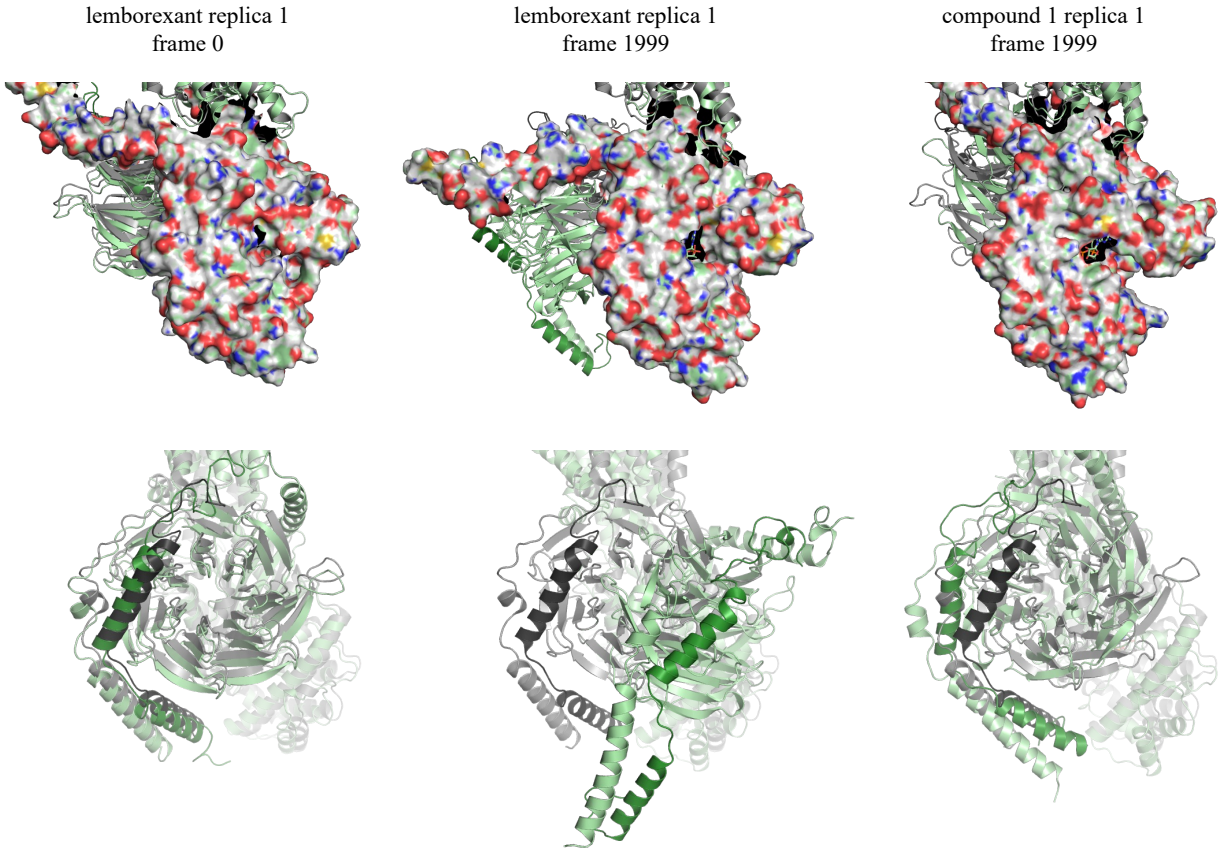

Figure S11. Changes in conformations of G protein subunits observed in MD simulations. (**Top**) A surface view of the full-length Gα subunit model (green) for the first frame of lemborexant replica 3 (**left**), the last frame of lemborexant replica 1 (**center**), and the last frame of compound 1 replica 1 (**right**) superposed on the templates (Gα—the 7SQ2 crystal structure; Gβ, Gγ and the receptor—the 7L1V cryo-EM structure) used for the homology modeling (gray). Gγ was marked in dark gray in the template structure and in dark green in the simulation-derived conformations. (Bottom) The side view from the Gβ and Gγ subunits. The movement of Gγ and the adjacent helical regions of Gβ during the Gα opening was observed in comparison to the template structure.

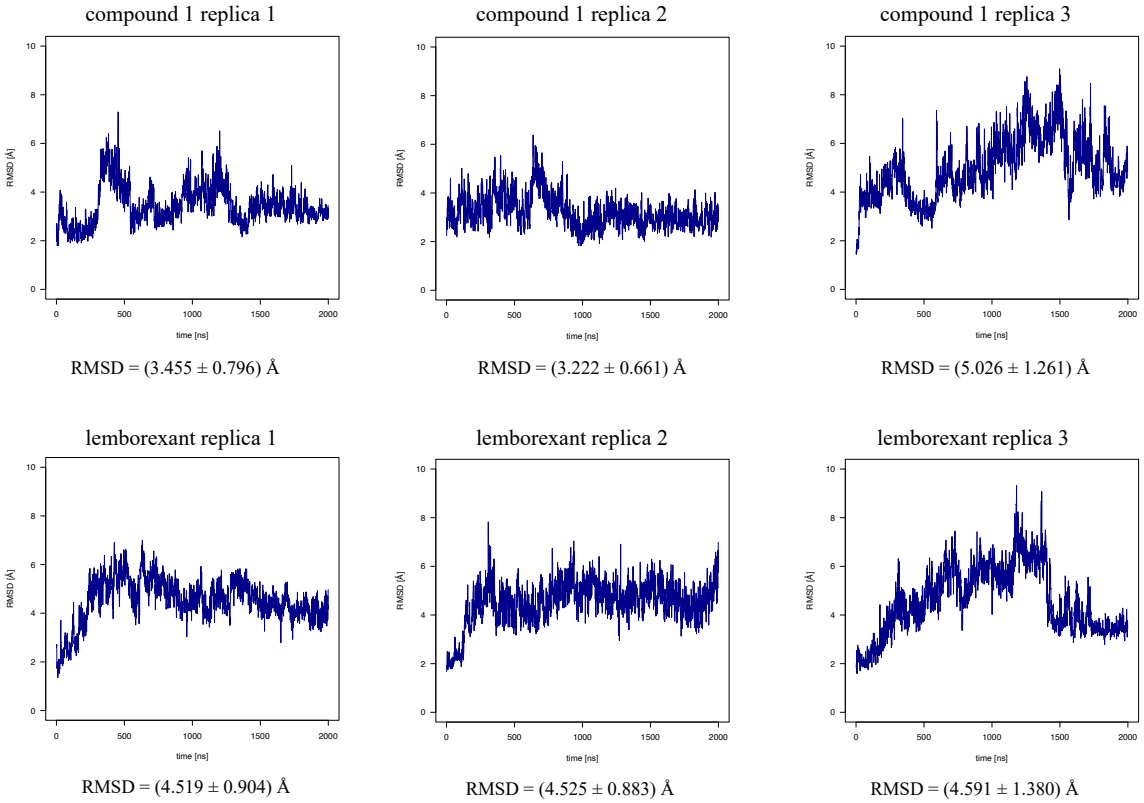

Figure S12. Fluctuations of the AHD domain in simulations. The RMSD plots and average RMSD fluctuations observed for AHD in compound 1 and lemborexant-including replicas.

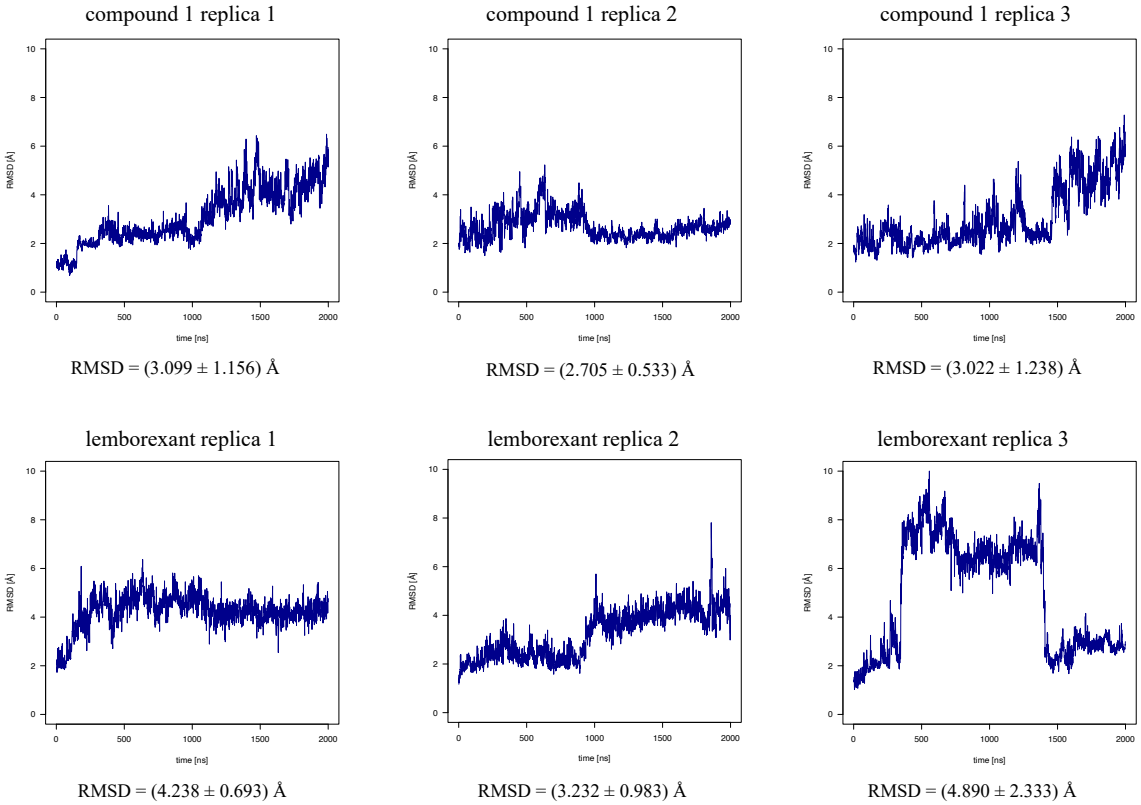

Figure S13. Fluctuations of GDP in simulations. The RMSD plots and average RMSD fluctuations observed for GDP in the compound 1 and lemborexant-including simulations.

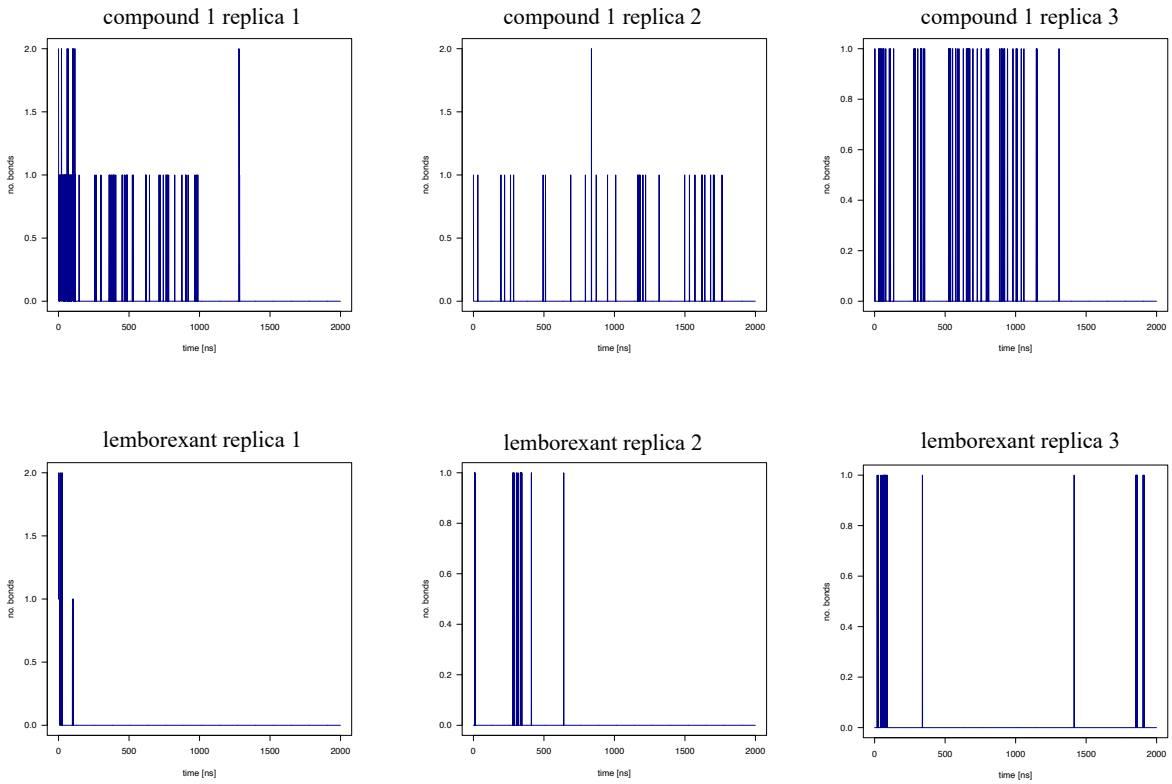

Figure S14. The formation of hydrogen bonds between GDP and R183$^{G.hfs2.02}$ in the compound 1 and lemborexant-including simulations. The hydrogen bond distance was specified as 4 Å, and the angle cut-off was 20º.

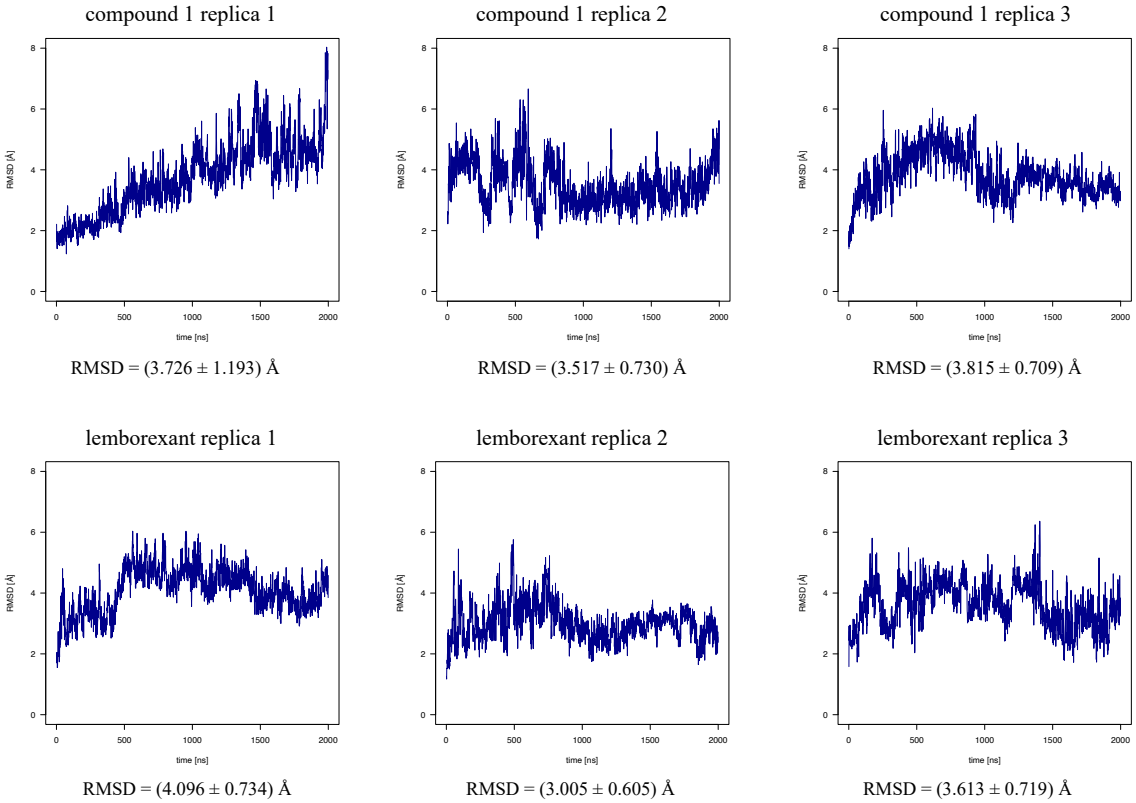

Figure S15. Fluctuations of the macroswitch I in simulations. The RMSD plots and average RMSD fluctuations observed for the macroswitch I in the compound 1 and lemborexant-including simulations.

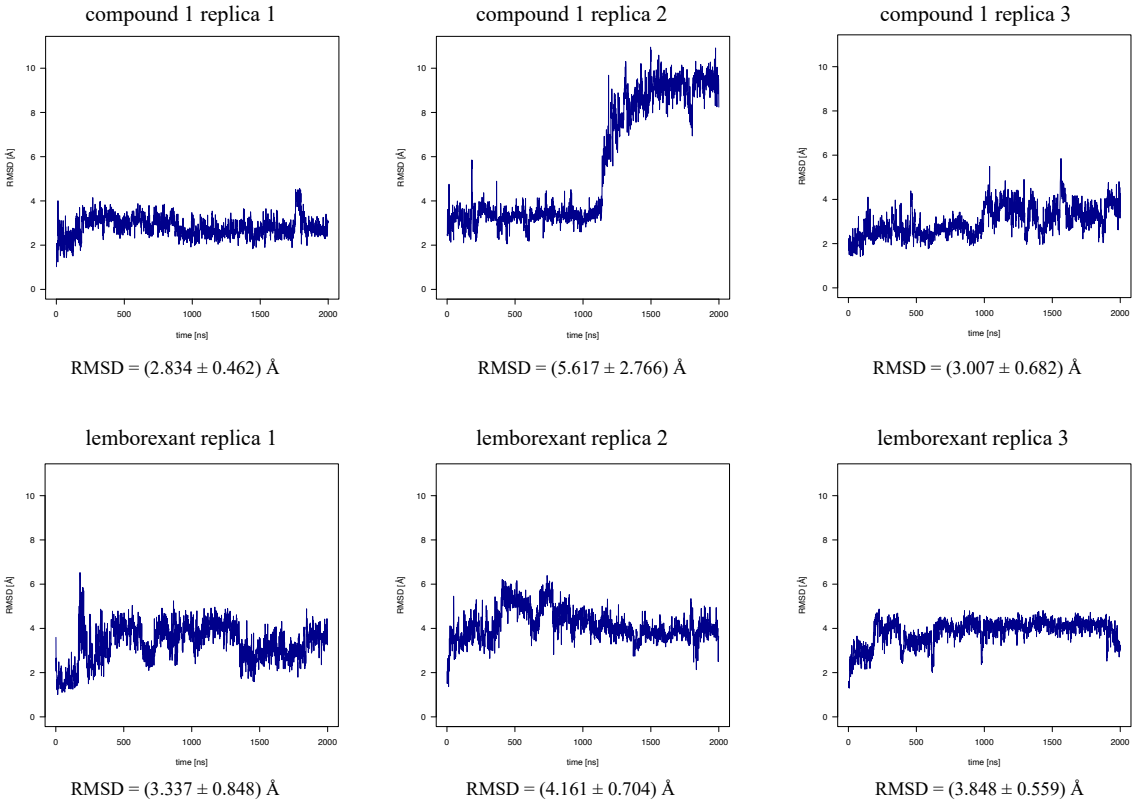

Figure S16. Fluctuations of the macroswitch III in simulations. The RMSD plots and average RMSD fluctuations observed for the macroswitch III in the compound 1 and lemborexant-including simulations.

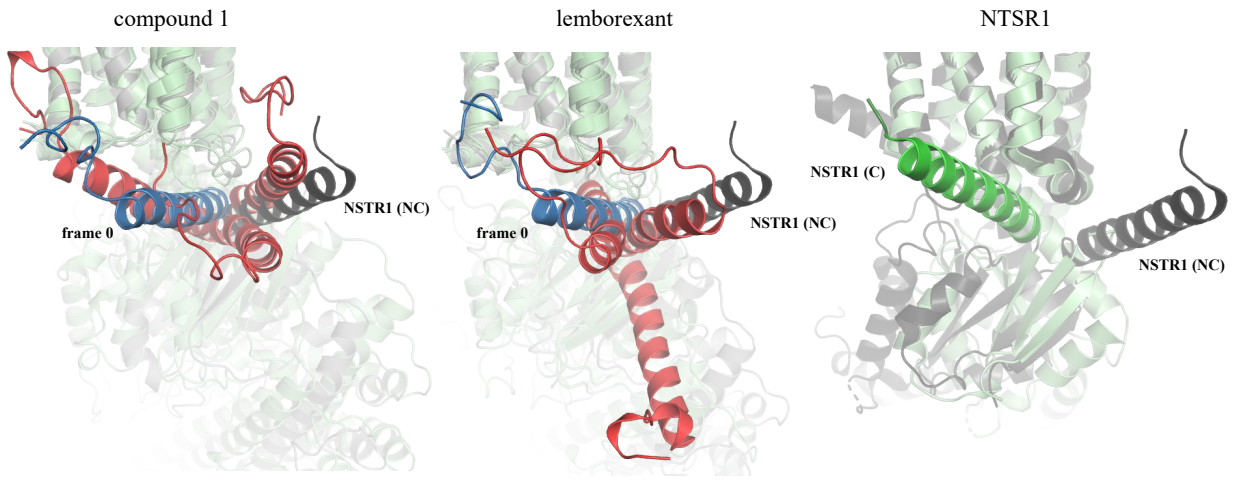

Figure S17. Changes in the orientation of N-terminal helices of Gα in the compound 1 and lemborexant-including simulations in comparison to known active-state NTSR1 structures from PDB. The first frame of the simulation was shown in gray with a blue N-terminal helix, and the final frame was shown in green with a red N-terminal helix. The changes in the lemborexant-including complexes resembled the active-like direction of changes in NTSR1 [13]. (**Right**) The two active states of NTSR1: 6OSA—gray and 6OS9—green. In the case of NTSR1, one fully active state (C, PDB ID: 6OS9 [4]) was preceded by the other one (NC, PDB ID: 6OSA [4]), with the N-terminal helix of Gα rotated by 45° counterclockwise with respect to the receptor main axis (right). The active-state structure of rhodopsin (6CMO) represented the fully active C state but with the N-terminal helix slightly moved to the intracellular side. The homology models used to generate the simulation systems all included the Gα N-terminal helix in between the NC and C states, slightly closer to the C state. At the end of the simulations, the same direction of changes towards the C state was observed only for one compound 1-including replica 1, which also demonstrated the most similarities to pre-opening state of Gα. However, for compound 1-including replica 3, the N-terminal helix moved towards the NC state. In the remaining lemborexant-including replicas, the N-terminal helix of Gα either remained as it was or moved to the bottom, not to the left as in 6OS9. This could suggest that the differences between the exerted effects of lemborexant and the classic agonist compound 1 on OX_2 could be due to the stabilization of slightly different conformational states of the OX_2–G protein multicomplex during activation.

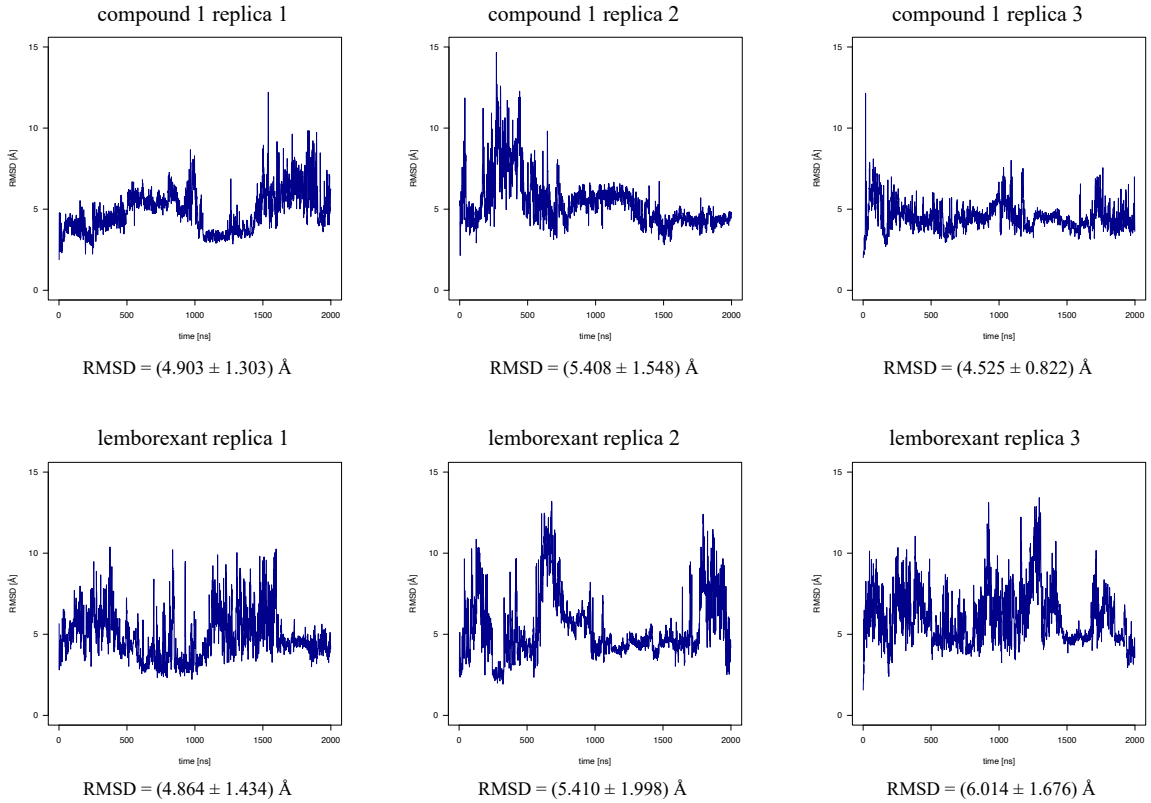

Figure S18. The RMSD plots and average RMSD fluctuations observed for ECL2 in the compound 1 and lemborexant-including simulations. The movement of ECL2 was also suggested when comparing the active-state (7L1V) and inactive-state (7XRR) structures, as it highly mobile in the former, and helical and arranged parallel to the lipid bilayer in the latter. The N-terminal helical region has been shown to be necessary for high-potency neuropeptide mediated activation of OX_2 [14]. In comparison to our previous MD simulations of OX_2 with mini-G_{sqi}, ECL2 closed even more quickly for the compound 1 simulations. More fluctuations were present in the lemborexant systems, and ECL2 closed more slowly when compared to compound 1.

References

1. *HCRTR1—Orexin/Hypocretin receptor type 1—Homo sapiens (Human) | UniProtKB | UniProt*. (2022, August 3). https://www.uniprot.org/uniprotkb/O43613/entry

2. *HCRTR2—Orexin receptor type 2—Homo sapiens (Human) | UniProtKB | UniProt*. (2022, October 12). https://www.uniprot.org/uniprotkb/O43614/entry

3. Hong, C., Byrne, N. J., Zamlynny, B., Tummala, S., Xiao, L., Shipman, J. M., Partridge, A. T., Minnick, C., Breslin, M. J., Rudd, M. T., Stachel, S. J., Rada, V. L., Kern, J. C., Armacost, K. A., Hollingsworth, S. A., O'Brien, J. A., Hall, D. L., McDonald, T. P., Strickland, C., … Hollenstein, K. (2021). Structures of active-state orexin receptor 2 rationalize peptide and small-molecule agonist recognition and receptor activation. *Nature Communications*, *12*(1), 815. https://doi.org/10.1038/s41467-021-21087-6

4. Kato, H. E., Zhang, Y., Hu, H., Suomivuori, C.-M., Kadji, F. M. N., Aoki, J., Krishna Kumar, K., Fonseca, R., Hilger, D., Huang, W., Latorraca, N. R., Inoue, A., Dror, R. O., Kobilka, B. K., & Skiniotis, G. (2019). Conformational transitions of a neurotensin receptor 1–Gi1 complex. *Nature*, *572*(7767), Article 7767. https://doi.org/10.1038/s41586-019-1337-6

5. Kang, Y., Kuybeda, O., de Waal, P. W., Mukherjee, S., Van Eps, N., Dutka, P., Zhou, X. E., Bartesaghi, A., Erramilli, S., Morizumi, T., Gu, X., Yin, Y., Liu, P., Jiang, Y., Meng, X., Zhao, G., Melcher, K., Ernst, O. P., Kossiakoff, A. A., … Xu, H. E. (2018). Cryo-EM structure of human rhodopsin bound to an inhibitory G protein. *Nature*, *558*(7711), Article 7711. https://doi.org/10.1038/s41586-018-0215-y

6. Ballesteros, J. A., & Weinstein, H. (1995). Integrated methods for the construction of three-dimensional models and computational probing of structure-function relations in G protein-coupled receptors. *Methods in Neurosciences*, *25*(C), 366–428. Scopus. https://doi.org/10.1016/S1043-9471(05)80049-7

7. Madeira, F., Pearce, M., Tivey, A. R. N., Basutkar, P., Lee, J., Edbali, O., Madhusoodanan, N., Kolesnikov, A., & Lopez, R. (2022). Search and sequence analysis tools services from EMBL-EBI in 2022. *Nucleic Acids Research*, *50*(W1), W276–W279. https://doi.org/10.1093/nar/gkac240

8. *GNAQ - Guanine nucleotide-binding protein G(q) subunit alpha—Homo sapiens (Human) | UniProtKB | UniProt*. (2022, December 14). https://www.uniprot.org/uniprotkb/P50148/entry

9. Waldo, G. L., Ricks, T. K., Hicks, S. N., Cheever, M. L., Kawano, T., Tsuboi, K., Wang, X., Montell, C., Kozasa, T., Sondek, J., & Harden, T. K. (2010). Kinetic Scaffolding Mediated by a Phospholipase C–β and Gq Signaling Complex. *Science*, *330*(6006), 974–980. https://doi.org/10.1126/science.1193438

10. Pándy-Szekeres, G., Esguerra, M., Hauser, A. S., Caroli, J., Munk, C., Pilger, S., Keserű, G. M., Kooistra, A. J., & Gloriam, D. E. (2022). The G protein database, GproteinDb. *Nucleic Acids Research*, *50*(D1), D518–D525. https://doi.org/10.1093/nar/gkab852

11. Calebiro, D., Koszegi, Z., Lanoiselée, Y., Miljus, T., & O'Brien, S. (2021). G protein-coupled receptor-G protein interactions: A single-molecule perspective. *Physiological Reviews*, *101*(3), 857–906. https://doi.org/10.1152/physrev.00021.2020

12. Ham, D., Ahn, D., Ashim, J., Cho, Y., Kim, H. R., Yu, W., & Chung, K. Y. (2021). Conformational switch that induces GDP release from Gi. *Journal of Structural Biology*, *213*(1), 107694. https://doi.org/10.1016/j.jsb.2020.107694

13. Ahn, D., Ham, D., & Chung, K. Y. (2021). The conformational transition during G protein-coupled receptor (GPCR) and G protein interaction. *Current Opinion in Structural Biology*, *69*, 117–123. https://doi.org/10.1016/j.sbi.2021.03.013

14. Yin, J., Babaoglu, K., Brautigam, C. A., Clark, L., Shao, Z., Scheuermann, T. H., Harrell, C. M., Gotter, A. L., Roecker, A. J., Winrow, C. J., Renger, J. J., Coleman, P. J., & Rosenbaum, D. M. (2016). Structure and ligand-binding mechanism of the human OX1 and OX2 orexin receptors. *Nature Structural & Molecular Biology*, *23*(4), Article 4. https://doi.org/10.1038/nsmb.3183